iomac
International Operational Modal Analysis Conference
11th International Operational Modal Analysis Conference
20 - 23 May 2025 | Rennes, France

# Stochastic modal analysis of pipe wall thinning structure based on Generative Adversarial Net (GAN) associated with interfacial roughness model

*Banri Yamamoto*[1], *and Soichiro Takata*[2]

[1] National Institute of Technology, Tokyo College, foot08232004@gmail.com
[2] National Institute of Technology, Tokyo College, takata@tokyo-ct.ac.jp

## ABSTRACT

Currently, buried water pipes cause burst accidents and water leakage, which is a social problem. The reasons for this are graphitization corrosion. The corroded pipe caused pipe wall thinning as the strength of the sectional area is decreased. Our previous research was proposed a diagnosis method based on the eigenfrequency change in the in-plane bending mode in the cylindrical shells. The eigenfrequency of the in-plane bending mode was directly proportional to the pipe thickness. However, the simulation model in the previous study could not sufficiently take into account the spatial inhomogeneity in the pipe model, because there are only a few image data of the dug up pipe wall thickness. In this study, we atempt the application to generative AI for corrosion image. The corrosion image samples generates from past dug up images of water pipe corrosion using by Generative Adversarial Nets (GAN), which is a generative artificial intelligence (AI). First, the correlation function fitting were conducted using a few image data of the dug up pipe wall thickness. Furthermore, the images for the GAN learning data were obtained based on interfacial roughness model. Moreover, the image generation was conducted using the GAN. Finaly, the fundumental operation test was perormed using finite elemnt method based on the generated corrosion image by GAN.

*Keywords: Generative Adversarial Net, Interfacial roughness model, Stochastic Modal Analysis*

## 1. INTRODUCTION

Currently, buried water pipes cause burst accidents and water leakage, which is a social problem. The reasons for this are graphitization corrosion. The corroded pipe caused pipe wall thinning as the strength of the sectional area is decreased. It is important to assess their condition using non-destructive testing, however, there are no effective measurement methods for buried situations, because they cannot be visually inspected [1-4]. In previous research, we proposed a diagnosis method based on the eigenfrequency change in the in-plane bending mode in the cylindrical shells [5]. The eigenfrequency

of the in-plane bending mode was directly proportional to the pipe thickness. Therefore, the inspection of a buried pipe is expected to be conducted using its vibration mode [5-6]. In the design of the threshold for discrimination, the simulation accuracy of finite element method is important. The actual pipe wall thickness exhibits spatially inhomogeneous characteristics because of the exposed corrosion environment. However, the simulation model in the previous study could not sufficiently take into account the spatial inhomogeneity in the pipe model, because there are only a few image data of the dug up pipe wall thickness [5].

In this study, we atempt the application to generative AI for corrosion image. The overall architecture is shown in **Figure 1**. First, correlation function fitting conducts using a few image data of the dug up pipe wall thickness. We apply curve fitting based on the interfacial roughness model, which is well done by modeling the facial roughness in III-V semiconductors [7]. The model was supposed to be the Gaussian correlation. By assuming a physical model, it is possible to provide a physical meaning and understanding for the generated corrosion images. Moreover, the feature analysis conducts focused on the two types of features in terms of roughness height and correlation length from the sample image data. In addition, the probability density functions of these two features are obtained by performing spatial random sampling. These probability density functions are used to evaluate the generative AI. Furthermore, the images for the GAN learning data obtain based on interfacial roughness model. Moreover, the image generation was conducted using the GAN. Finaly, the fundumental operation test perorms using finite elemnt method based on the generated corrosion image by GAN.

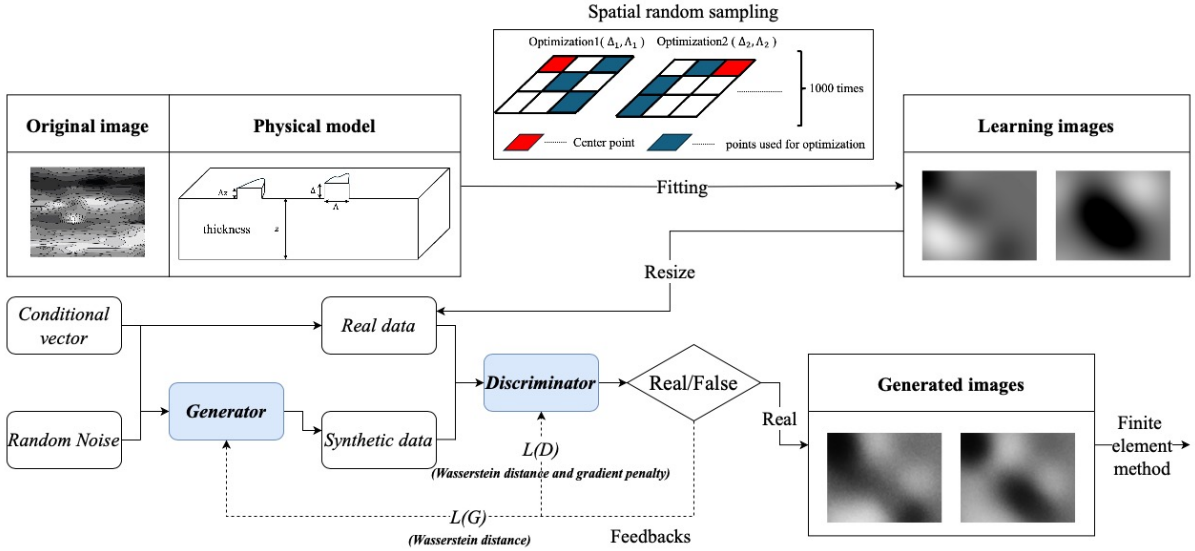


**Figure 1.** The process from image generation to the finite element method.

## 2. GENERATION OF TRAINING IMAGES USED FOR GENERATIVE AI

### 2.1. Data used for the generation of training images

The main water thickness distribution after graphitization corrosion as researched by Smiths is shown in **Figure 2**. These data were obtained by measuring the outer wall thickness of the water main with a length of 3.54 m and a caliber of 1070 mm using a Vernier scale. The horizontal and vertical axes represent the length of the pipe (0-3.54 m) and the angle (0°- 360°), respectively. The color bar indicates the main water thickness which ranges from 27 mm to 35 mm. Here, light colors (closer to white) indicate thicker sections of the pipe, while darker colors (closer to black) indicate thinner sections. In this study, we applied statistical analysis and parameter estimation to a physical model of a corrosion surface, using image data as input, and are applied, classical sampling was used to obtain training data.

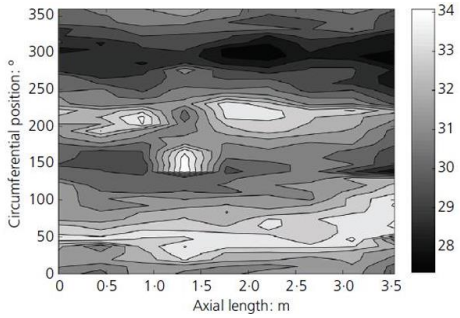


**Figurę 2.** Thickness distribution of graphitized water main [1] .

## 2.2. Model construction for training data using interface roughness model

### *2.2.1. Interface roughness model*

In this study, the physical model of the corrosion surface assumes interface roughness model [7]. First, using the pipe thickness distribution data shown in **Figure 2**, the nonlinear least squares method was applied to the interface roughness model. The interface roughness model used in this study was model for expression of surface roughness distribution in group III-V semiconductor heterostructures. In this model, the relative distance vectors from a certain point are $\boldsymbol{r}$ and $\boldsymbol{r}'$, respectively, and the deviations from the mean pipe thickness at those positions are $\Delta z(\boldsymbol{r})$ and $\Delta z(\boldsymbol{r}')$, respectively. The mean value of the product of these deviations is a model that assumes a Gaussian correlation function between roughness height $\Delta$ and size $\Lambda$, as expressed in Eq. (1) and **Figure 3**.

$$\langle \Delta z(\boldsymbol{r}) \cdot \Delta z(\boldsymbol{r}') \rangle = \Delta^2 \exp\left( -\frac{(\boldsymbol{r} - \boldsymbol{r}')^2}{\Lambda^2} \right) \tag{1}$$

In addition, as a statistical characteristic of this model, the statistical distribution of the roughness height and size was revealed by spatial random sampling.

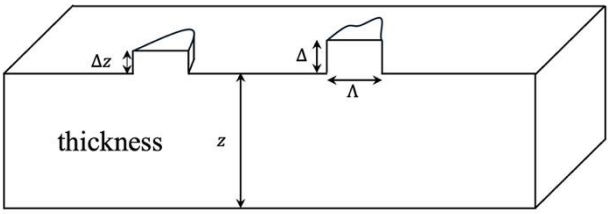


**Figure 3.** Schematic diagram of the interface roughness model.

### *2.2.2. Identification result*

Assuming that the data shown in **Figure 2** obeys Eq. (1) , 5000 data points were taken from the image, and the parameters were obtained using the Levenberg-Marquardt algorithm as a nonlinear least squares problem. For this analysis, the initial values are set to $\Delta$ for the maximum value of the correlation function and $\Lambda = 1$. Any point in the image was a representative point. The correlation function at the relative distance from the representative point was calculated, and the parameters were obtained to minimize the squared error using Eq. (1). As a result, an example of an estimated value was $\Delta \approx 1.514$, $\Lambda \approx 136$. **Figure 4** shows an example of a curve fitted correlation function that applies nonlinear least squares. The horizontal and vertical axes show the relative distance of the spatial coordinates and the correlation function, respectively. The black point and blue solid line show 5000 data points from the image and the curve fitted line, respectively. The curve fitted results expressed an outline of the correlation function calculated from the image data.

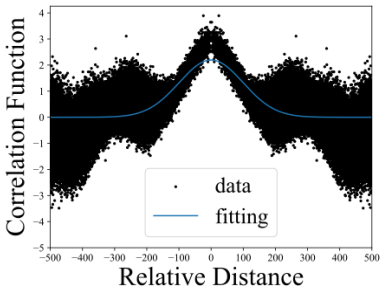


**Figure 4.** The spatial cross-correlation function.

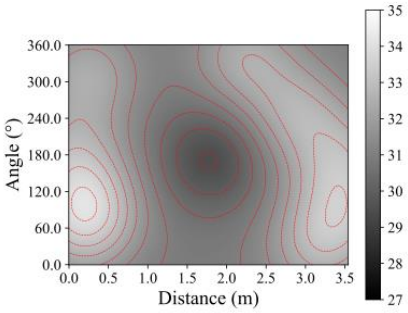


**Figure 5.** The image following interfacial roughness model.

**Figure 5** presents the pipe thickness distribution, where the horizontal and vertical axes represent pipe length and angle. Darker shading indicates more corrosion, with a central thinning area of about 50 cm in diameter and 5 mm in depth. The corrosion pattern reflects macro cell corrosion. The image size is 583×742 (total 432,586 pixels). **Figures 6,7** present histograms from 1,000 estimations of roughness parameters (Δ, Λ) obtained by spatial random sampling. A Gaussian mixture model was fitted, with the optimal number of distributions determined by the Bayesian Information Criterion (BIC). The Kolmogorov-Smirnov test confirmed normality for roughness height (p value = 0.15926), while roughness size followed a bimodal distribution. These statistics were used to evaluate AI-generated images.

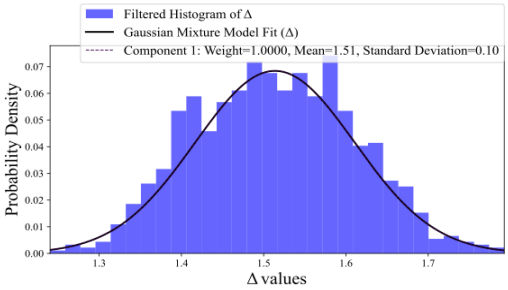


**Figure 6.** Probability density distribution of roughness height.

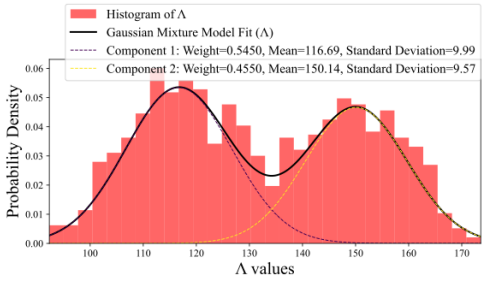


**Figure 7.** Probability density distribution of roughness size.

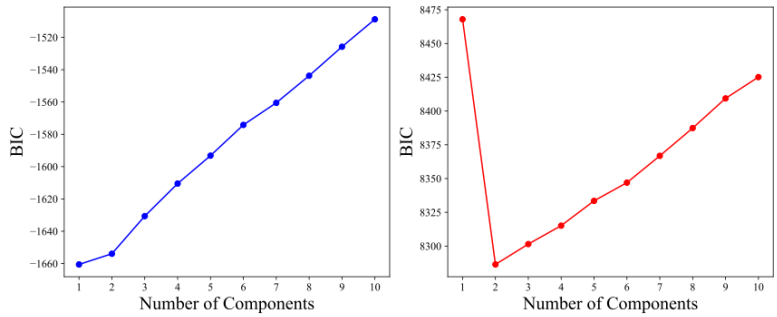


**Figure 8.** Bayesian Information Criterion (BIC) in number of components.

## 3. THE UTILIZATION AND EVALUATION OF GENERATIVE AI

### 3.1. Generative model

The method of Conditional Wasserstein Generative Adversarial Networks with gradient penalty (CWGAN-gp) were applied to the used generative model [8].

### *3.1.1. Generative Adversarial Networks*

GANs generates images that compete with two neural networks. One network is a generator that generates images, and the other is a discriminator that identifies real images by understanding their distribution and features. During training, the generator proceeds with learning to generate images in which the discriminator identifies real images. The discriminator learns to identify a real image. It is called "Adversarial" from deceiving each other in this way and trying to distinguish. The learning of the generator and discriminator was formulated as a zero-sum game, and the loss function in the optimization problems of the GAN is given by Eq. (2).

$$\min_{G}\max_{D} L(D,G) = \mathrm{E}_{\boldsymbol{x}\sim p_r}[\ln D(\boldsymbol{x})] + \mathrm{E}_{\boldsymbol{z}\sim p_z}\left[\ln\left(1 - D\left(G(\boldsymbol{z})\right)\right)\right] \tag{2}$$

where $\boldsymbol{x}\sim p_r$ and $\boldsymbol{z}\sim p_z$ are the distributions of real data and input noise respectively, and $D(\cdot)$ is the identification result of the discriminator and $G(\cdot)$ is the input of the generator. When the generator and the discriminator parameters are $\theta_G$ and $\theta_D$ respectively, the optimization problem has a destination for the generator and the discriminator parameters called Nash equilibrium.

### *3.1.2. Conditional Wasserstein Generative Adversarial Networks with gradient pernalty*

In addition to GAN, the conditional vector, Wasserstein distance and gradient penalty terms were used. It is called CWGAN-gp. The Earthmover (EM) distance (also called Wasserstein-1) is defined in Eq. (3).

$$W(p_r, p_g) = \inf_{\gamma\in\Pi(p_r,p_g)} \mathrm{E}_{(x,y)\sim\gamma}[\|x - y\|] \tag{3}$$

where $\Pi(p_r, p_g)$ denote the set of all joint distributions $\gamma(x,y)$ whose marginals are respectively $p_r$ and the generated image distribution $p_g$. The loss function in the optimization problems of the WGAN-gp is given by Eq. (4).

$$L = \mathrm{E}_{\tilde{\boldsymbol{x}}\sim p_g}[D(\tilde{\boldsymbol{x}})] - \mathrm{E}_{\boldsymbol{x}\sim p_r}[D(\boldsymbol{x})] + \lambda \mathrm{E}_{\hat{\boldsymbol{x}}\sim p_{\hat{x}}}[(\|\nabla_{\hat{\boldsymbol{x}}} D(\hat{\boldsymbol{x}})\| - 1)^2] \tag{4}$$

where $\hat{\boldsymbol{x}}\sim p_{\hat{\boldsymbol{x}}}$ is defined as a uniformly sampled value along a line between any pair of points on $p_r$ and $p_g$ and $D(\cdot)$ is not the identification result value but the measuring value of Wasserstein distance. The conditional vector is added with WGAN-gp, it is called CWGAN-gp.

### *3.1.3. Conditional vector*

Here, the method for generating the conditional vector, given the WGAN-gp, is described. This model follows the interface roughness model and provides the physical constraint. Therefore, the highest potential is given by the difference between the thickest and thinnest pipes, as shown in Eq. (5).

$$V(\boldsymbol{R}) \approx -V_0 \delta w(\boldsymbol{R}) \tag{5}$$

where $\boldsymbol{R}$ denotes the correlation distance vector, and $\delta w(\cdot)$ denotes the thickness difference at a correlation distance vector.

In addition, the buried environment must be considered, as the focus is on the corrosion of the water main. Therefore, from the physical aspect, five items were calculated as follows: buried year, corrosion speed (depends on NaCl concentration and dissolved oxygen concentration), soil pH, number of corrosions (depends on soil moisture content) and highest potential from the statistical aspect, two items were calculated the tendency of roughness height and roughness size. In total, seven items were calculated based on the following criterion. The conditional vector is generated as shown in **Figure 9**.

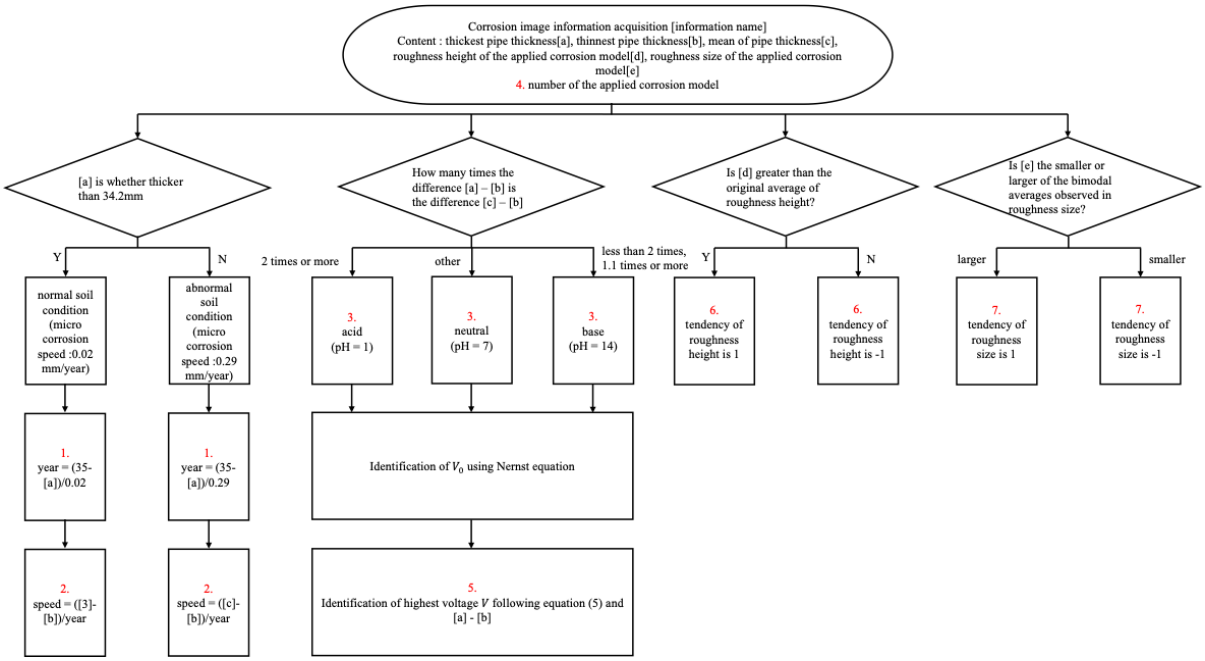


**Figure 9.** Flow chart of generating conditional vector (red number is label of conditional vector).

1. Buried year: Buried year was calculated to determine whether the soil is normal or abnormal.

2. Corrosion speed (macro cell corrosion): It depends on the NaCl and dissolved oxygen concentration.

3. Soil pH: Soil pH was limited to three types (acidic (pH = 1), neutral (pH = 7), and basic (pH = 14)).

4. Number of corrosion: This depends on soil moisture content.

5. Highest potential: From Eq. (5), $V_0$ must be calculated, as it was assumed that $V_0$ followed the Nernst equation (Eq. (6)).

$$V_0 = E^\circ + \frac{RT}{zF} \ln \frac{a_{Ox}}{a_{Red}} \tag{6}$$

where $E^\circ$ denotes the standard potential of iron ($E^\circ = -0.440$ V), $R$ denotes gas constant ($R \approx 8.31$ $m^2 \cdot kg/s^2 \cdot K \cdot mol$), $T$ denotes the absolute temperature ($T = 298.15$ K), $z$ denotes the number of moving electrons ($z = 2$), $F$ denotes Faraday constant ($F \approx 9.65 \times 10^5$ c/mol), $a_{Ox}$ denotes the activity of the oxidant ($a_{Ox} = [\mathrm{Ox}]$), $a_{Red}$ denotes the activity of reductant ($a_{Red} = 1$).

6. Tendency of roughness height: It was determined from the characteristic shown in **Figure 6**.

7. Tendency of roughness size: It was determined from the characteristic shown in **Figure 7**.

**Figure 10** and **Table 1** show examples of the image and conditional vectors, respectively.

### 3.2. Statistical evaluation

A statistical evaluation of the generated images was performed. However, the original image size was too large for direct import into the FEM. Generating high-resolution images using CWGAN-gp would be costly if the image size was too large. To address this, the original image was resized to 1/10th of its length and width using a Lanczos filter, a commonly used resampling method. After resizing, no significant differences were observed in the statistical characteristics of the roughness height between the resized CWGAN-gp-generated images. However, differences were observed in roughness size. **Figure 11** and **Figure 12** show the probability density distribution of the roughness size after resizing and generation by CWGAN-gp, respectively. Resizing caused the bimodality distribution of the roughness size in the original image to disappear. However, this bimodal characteristic was restored by the CWGAN-gp-generated images.

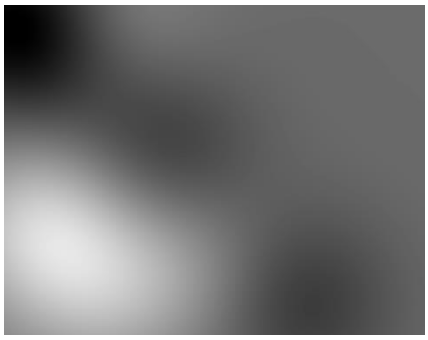

**Figure 10.** Corrosion image generated by CWGAN-gp.

**Table 1.** Generated conditonal vector of Figure 10.

| Item | Value |
|---|---|
| Buried year | 14 |
| Corrosión speed | 0.1220595 |
| Soil pH | 14 (base) |
| Number of corrosion | 2 |
| Highest potential | 1.22971465 |
| Tendency of roughness height | -1 |
| Tendency of roughness size | 1 |

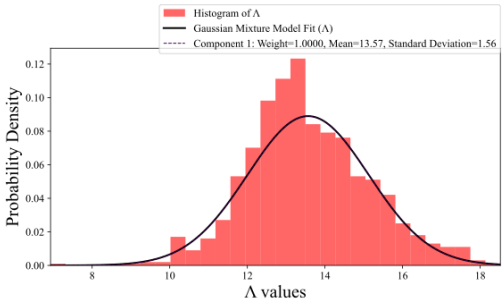


**Figure 11.** Probability density distribution of roughness size after resizing 1/10.

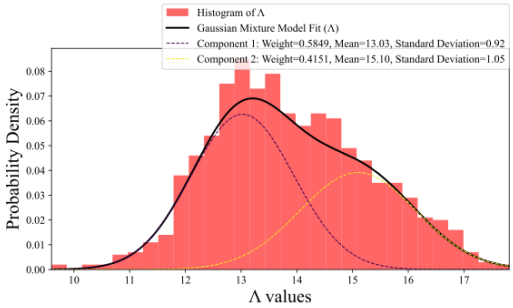


**Figure 12.** Probability density distribution of roughness size after generation by CWGAN-gp.

## 4. STOCHASTIC MODAL ANALYSIS USING GENERETED CORROSION IMAGE

The fundamental operation test was conducted using the general finite element method (FEM) simulation tool (ANSYS 2024 R1, Cybernet.co.,). The FEM model is shown in **Figure 13**.

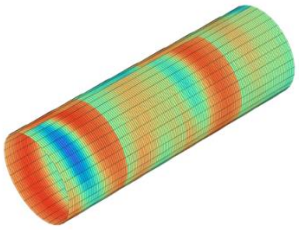

**Figure 13.** Finite element model which has distributed deteriorated regions.

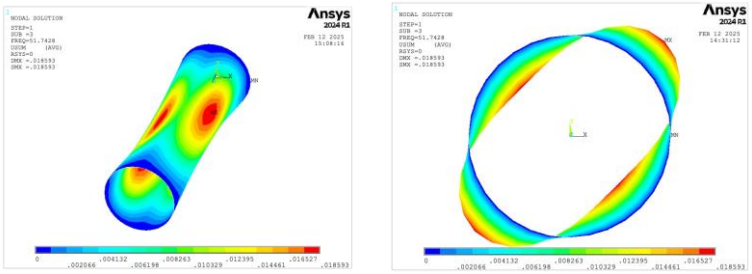


**Figure 14.** The in-plane bending mode in the finite element model.

A 7 m length main water pipe was created using two generated images. Using this model which is constructed from shell element (shell 181) and clamped-clamped boundary, we performed a modal analysis to confirm the in-plane bending vibration of the cylindrical shell. The result of mode shape of in-plane bending mode is shown in **Figure 14**, and the eigen frequency was 51.7428 Hz. Thus, the fundamental operation of the proposed prototype was confirmed by the modal analysis using a CWGAN-gp-genetared image. Its statistical consideration of the modal analysis based on the large number of CWGAN-gp-genetared image is future work.

## 5. CONCLUSION

In this paper, we were discussed the stochastic modal analysis using the GAN-generated-image. The following results were obtained.

(1) The corrosion image generation method was established based on the CWGAN-gp associated with the interfacial roughness model fitting and the condition vector generation based on the image analysis.
(2) The fundumental operation test of modal analysis using a CWGAN-gp-generated image was performed.


## ACKNOWLEDGEMENTS

This work was supported by JST Grant Number JPMJPF2115.


## REFERENCES


[1] A. Rainer, T. F. Capell, N. Clay-Michael, M. Demetriou, T. S. Evans, D. Jesson, M. Mulheron, L. Scudder, and P. A. Smith, What does NDE need to achieve for cast iron pipe networks?, Infrastructure Asset Management, ICE, 42(2) 68-82, DOI: 10.1680/jinam.16.00020, 2017.

[2] H. Mohebbi, D. A. Jesson, M. J. Mulheron, and P. A. Smith, The fracture and fatigue properties of cast irons used for trunk mains in the water industry, Materials Science and Engineering A-Structural Materials Properties Microstructure and Processing, 527, 5915-5923, DOI: 10.1016/j.msea.2010.05.071, 2010.

[3] H. M. S. Belmonte, M. Mulheron, and P. A. Smith Weibull analysis, extrapolations and implications for condition assessment of cast iron water mains, Fatigue & Fracture of Engineering Materials & Structures, 30, 964-990, DOI: 10.1111/j.1460-2695.2007.01167.x, 2007.

[4] K. Atkinson, J.T. Whiter, P. A. Smith, and M. Mulheron, Failure of small diameter cast iron pipes, Urban Water, 4(3), 263-271 DOI: 10.1016/S1462-0758(02)00004-3, 2002.

[5] S. Takata, H. Inoue, and S. Shinoda, Proposal of the pipe diagnosis method using in-plane bending vibration of cylindrical shell, Transactions of the JSME (in Japanese), 84(861), DOI:10.1299/transjsme.17-00522, 2018.

[6] N. Watanabe, S. Takata, and K. Toyoshima, Experimental modal analysis of in-plane bending mode using actual water main network, INTER-NOISE and NOISE-CON Congress and Conference Proceedings, 270(5), 6482-6492, DOI: 10.3397/in_2024_3769, 2024.

[7] H. Casella, and J. W. Wilkins, Splitting of the excitonic peak in quantum wells with inter facial roughness, Physical Review B, Vol. 58, No. 24, 1998.

[8] H. Wang, J. Bi, M. Hua, K. Yan, and A. Afshari, Semi-supervised CWGAN-GP modeling for AHU AFDD with high-quality synthetic data filtering mechanism, Building and Environment, Vol. 267, Part A, 2024.